

# Prospecting for cavities by seismic tomography techniques: The case of Akrotiri archaeological site, Thera Island, Greece

Ioannis F. Louis\*, *Geophysics & Geothermics Dpt., University of Athens, Panepistimiopolis Ilisia 15784, Greece.*

## Abstract

Cross-shaft seismic tomography experiments were performed at Akrotiri archaeological excavation area on Thera Island to image subsurface man-made cavities encountered in the basement rock. Seismic caps were used as downhole sources and a 12-channel geophone cable provided the downhole receivers. The seismic data were processed with a traveltimes tomography package to produce a velocity model. The cross-shaft velocity models exhibit rapid lateral and vertical velocity changes that are not resolved by surface methods. The cross-shaft tomographic images revealed low velocity structures attributed to prehistoric tombs.

## Introduction

In crosshole seismic tomography, seismic sources located in a well are shot into receivers located in a nearby well. The travel times of the first arrivals are used to produce a tomographic velocity cross-section of the subsurface between the two wells (Bregman et al., 1989; Calnan and Schuster, 1989; Lines and LaFehr, 1989; McMechan et al., 1987). Crosshole tomography provides better resolution than VSP or RVSP since most of the energy does not travel through the highly attenuating near surface layer and the travel distances are shorter. In addition, the resolution of crosshole tomography is not depth limited since most of the energy travels between the wells.



Figure 1. Multi-storeyed buildings and magnificent wall paintings were unveiled from excavations.

Crosswell seismic investigations were carried out at Akrotiri archaeological site, which is one of the most important prehistoric settlements of the Aegean. The first habitation at the site dates from the Late Neolithic times (at least the 4th

millennium B.C.). During the Early Bronze Age (3rd millennium B.C.), a sizeable settlement was founded, extended and gradually developed into one of the main urban centres and ports of the Aegean. The large extent of the settlement (ca. 20 hectares), the elaborate drainage system, the sophisticated multi-storeyed buildings (Figure 1) with the magnificent wall paintings, furniture and vessels, show its great development and prosperity.

The town's life came to an abrupt end in the last quarter of the 17th century B.C. when the inhabitants were obliged to abandon it as a result of severe earthquakes. The eruption followed. The volcanic materials covered the entire island and the town itself. These materials, however, have protected up to date the buildings and their contents, just like in Pompeii. Professor Sp. Marinatos began systematic excavations in 1967 under the auspices of the Archaeological Society at Athens. Since his death in 1974, the excavations have been continued under the direction of Professor Ch. Doumas.

Currently, the old monuments protective roof cover at Akrotiri is being replaced by a new elaborate and environment friendly construction. The new construction will be supported by 95 pillars embedded in an equal number of drilled shafts filled with concrete. The foundation shafts (1.2 meters in diameter and 8 meters depth) are opened up in the pyroclastic volcanic formation basement rock (figure 2).

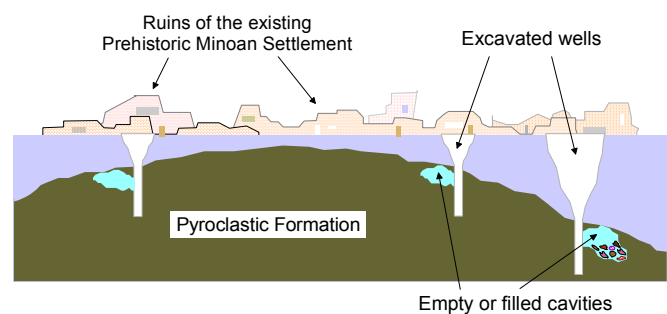


Figure 2. Sketch diagram of the excavated shafts with cavities in their walls.

The ceiling of the pyroclastic formation was found at depths varying between 2 and 15 meters below the ground surface where Prehistoric Minoan settlement is situated (figure 2).

Man-made cavities appeared in the walls of some foundation shafts during their excavation. Some of them were empty while others were filled or half filled with stones, ceramics

## Detection of cavities with crosshole seismics



Figure 3. The monuments protective roof cover and the field work area. In the left foreground the fireman charging shot holes in a transmitting shaft.



Figure 4. Receiving shaft: Putting geophones in the pyroclastic formation basement rock.

etc. According to the excavations findings they probably concern ancient prehistoric tombs excavated on the slopes of the pyroclastic basement rock. Seismic cross-shaft experiments were performed to detect them because their presence might affect the construction response during an earthquake.

### The experiments

Since the target of prospect is buried under a thick layer of ruins it was evident that surface seismic investigations would be incapable of detecting voids superimposed by such complex structures. This is due to the limitations, inherent in the physics of the method, where receivers pick up all the returns such as large reflections from many objects (ruins) in different positions. Consequently any, subsequent, received signal from the target will be attenuated. Moreover, the use of surface seismic sources would damage the archaeological monuments.

The existence of the excavated foundation shafts was an excellent opportunity to apply the crosshole seismic tomography technique. The crosshole tomographic experiments were performed in 10 locations between pairs of shafts. They comprise sources located in one shaft (figure 5) transmitting into receivers located in the neighbor shaft (hole to hole).

A 12-channel geophone cable served as the receiver. The space between receiver stations was 0.5 meters. The sources used in this experiment were seismic cap charges fired at 0.5 meters intervals from bottom to top of the shaft. Due to the short shaft-to-shaft distances the seismic cap provided high quality data without damaging the shaft. The seismic signals from all the stations were transmitted uphole simultaneously through tow leaders and recorded with a surface recording system.

### Data Analysis and Processing

Twelve shots ranging from bottom to top of each shooting shaft were recorded for each receiver station.

In crosshole transmission tomography, the first-arrival P-waves are used to produce a velocity cross-section. Therefore, the precision of the travel time measurement is vital to the resolution of the final velocity model. Since the S/N ratio of the data is good, an automatic picking program based in threshold technique was used to pick the first-arrival times. The precision of the picks is approximately 0.125 ms.

Tomographic imaging is based on ray theory. The region bordered by the two boreholes is divided into rectangular cells or pixels. The velocity of each cell is assumed to be constant and unknown.

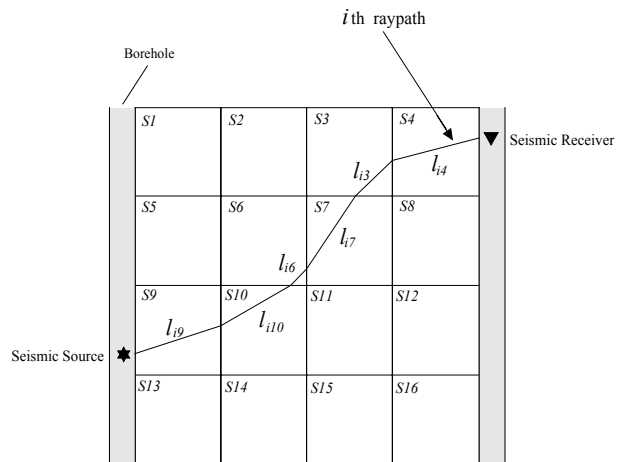


Figure 5. Schematic illustration of ray paths through a cell slowness model (from Berryman, 1991).

## Detection of cavities with crosshole seismics

Referring to Figure 5, let  $t_i$  be the first-arrival travel time for the  $i$ th ray,  $l_{ij}$  be the distance travelled across the  $j$ th cell by the  $i$ th ray, and  $s_j$  be the slowness of the  $j$ th cell (slowness is the inverse of velocity). If  $P_i$  be the Fermat ray path connecting the  $i$ th source-receiver pair, neglecting observation errors, we can write

$$\int_{P_i} s(x) \cdot dl^{P_i} = t_i, \quad i = 1, \dots, m \quad (1)$$

Given a model with  $N$  cells with the  $j$ th cell having constant slowness  $s_j$ , (1) can then be written

$$t_i = \sum_{j=1}^N l_{ij} s_j \quad (2)$$

Note that for any given  $i$ , the ray path lengths  $l_{ij}$  are zero for most cells  $j$ , as a given ray path will in general intersect only a few of the cells in the model. We can rewrite equation (2) in matrix notation by defining the column vectors  $s$  and  $t$  and the matrix  $M$  as follows:

$$\mathbf{s} = \begin{bmatrix} s_1 \\ s_2 \\ \vdots \\ s_n \end{bmatrix} \quad \mathbf{t} = \begin{bmatrix} t_1 \\ t_2 \\ \vdots \\ t_n \end{bmatrix} \quad \mathbf{M} = \begin{bmatrix} l_{11} & l_{12} & \dots & l_{1n} \\ l_{21} & l_{22} & \dots & l_{2n} \\ \vdots & \vdots & \ddots & \vdots \\ l_{m1} & l_{m2} & \dots & l_{mn} \end{bmatrix}$$

Equation (2) then becomes the basic equation of forward modelling for ray equation analysis:

$$\mathbf{M}\mathbf{s} = \mathbf{t}$$

Given the travel times vector  $\mathbf{t}$  and the raypaths matrix  $\mathbf{M}$ , we need to solve for the slowness vector  $\mathbf{s}$ . The number of rows of  $\mathbf{M}$  equals the number of rays (first-arrival time picks). The number of columns of  $\mathbf{M}$  equals the number of pixels (cells) in the image. For example, for the experiment between shafts, we had

Number of pixels = 12 X 25 = 300

Number of rays = 144

To invert the seismic data we used CAT3D package developed by OGS (Vesnaver, 1996). The inversion algorithm is robust with respect to noise contaminating the data, and does not depend strongly on the *a priori* information as most conventional algorithms.

The iterative method SIRT (Simultaneous Iterative Reconstruction Technique) was used for the inversion. The algorithm has two main components: Tracing the rays to obtain  $\mathbf{M}$  (raypaths) and solving for the  $\mathbf{s}$  (SIRT). The processing is taking place in a SUN spark workstation. Pixel size was chosen to be 0.6 meters vertically and 0.6 meters horizontally leading to a total of 300 pixels. The first iteration was done with an initial guess of constant velocity of 1500

m/s. The regularized SIRT was run through 5 iterations and the obtained velocity field was used again as an initial velocity model to obtain the final velocity field after 10 more iterations.

Figure 6 shows the ray coverage for the investigated area between shafts  $\Phi 43A$  and  $\Phi 43$ . The measure of ray coverage or ray density is a popular indicator to estimate the inversion reliability. This indicator is measured here as the number of rays crossing each pixel. Although it can be computed very easily, it is considered rather a poor indicator of the local reliability, because it does not distinguish linearly dependant from independent rays. Singular value analysis and null space energy indicators are used today along with ray density to estimate the reliability of the solution.

Figure 7 shows the final velocity field (model) obtained from the inversion of first-arrival times. The major events in the velocity-depth section are identified as follows:

1. The pyroclastic formation basement with variable seismic velocities attributed to volcanic material.
2. The two characteristic low velocity structures L1 and L2 attributed to verified cavities.

Figures 8 and 9 show respectively the ray coverage and the final velocity model obtained from the uphole seismic tomography experiment between shaft  $\Phi 22$  and the ground surface. The major events are identified as follows:

1. The surface layer with low velocity variations (300 - 700 m/s) attributed to a volcanic tephra layer
2. An intermediate velocity zone (600 - 1200 m/s) attributed to the ruins layer and
3. The pyroclastic formation basement layer with the low velocity structure L attributed to the verified cavity.

Unfortunately, coverage near the top and bottom of the shafts is poor (Figure 6). The lack of ray coverage in the upper part area (Figure 6) can be overcome by combining crosshole seismic with Vertical Seismic Profiling (VSP) and/or Reverse Vertical Seismic Profiling (RVSP) techniques. Concerning the lack of information for the lower part, the wells need to be drilled considerably deeper than the zone of interest.

### Conclusions

Crosshole seismic tomography experiments can produce higher resolution subsurface images than surface seismic or resistivity data. Crosshole tomography provides even higher resolution cross-sections than surface methods and can potentially resolve smaller structures. This, in large part, is due to less attenuation of high frequencies in the crosshole data. Unlike RVSP and surface seismic where all the waves need to travel to the surface, most of the crosshole energy travels only between the wells. Therefore, the subsurface images produced by crosshole tomography will maintain the same high resolution as the depth increases, while the images

## Detection of cavities with crosshole seismics

produced by RSVP or surface seismic may lack in resolution. In addition, crosshole tomography can distinguish both lateral

and vertical velocity changes, which can provide valuable information about rock properties.

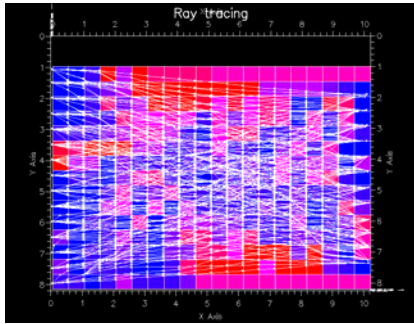


Figure 6. Ray coverage area between shafts Φ43A and Φ43.

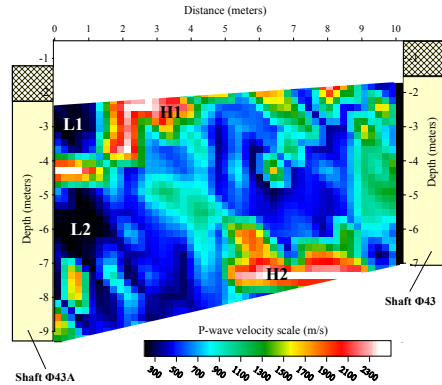


Figure 7. Seismic velocity image obtained from cross-shaft seismic tomography experiment. Cavities are shown as low velocity structures L1 and L2.

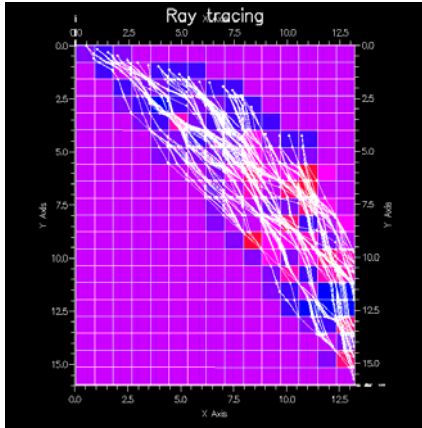


Figure 8. Ray coverage area from the uphole experiment between shaft Φ22 and the ground surface.

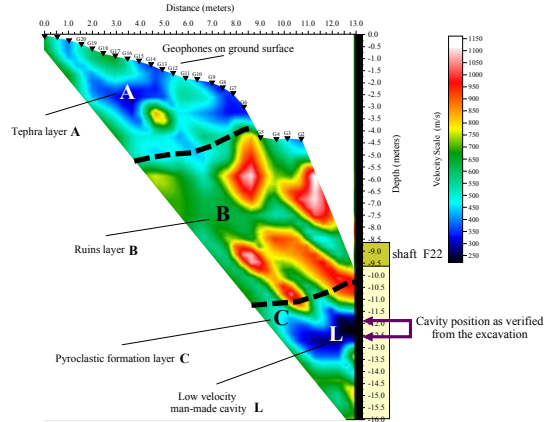


Figure 9. Seismic velocity image obtained from the uphole seismic tomography experiment. Cavity is shown as low velocity structure L.

### References

Berryman, J. G., 1991, Lecture Notes on Nonlinear Inversion and Tomography: LLNL, Livermore, CA.

Bregman, N. D., Bailey, R. C., and Chapman, C. H., 1989, Crosshole seismic tomography: *Geophysics*, 54, 200-215

Calnan, C., and Schuster, G. T., 1989, Reflection and transmission cross-well tomography: Presented at the 59<sup>th</sup> Ann. Internat. Mtg., Soc. Expl. Geophys., Expanded Abstracts, 908-911.

Lines, L. R., and LaFehr, E. D., 1989, Tomographic modeling of a cross-borehole data set: *Geophysics*, 54, 1249-1257.

Louis, I. F., 2001, Geophysical Investigations within the frameworks of exhibition and replacement of the old roof cover at Akrotiri-Thera. Archaeological excavations area. Technical Report submitted to the Archaeological Society at Athens

McMechan, G. A., Harris, J. M., and Anderson, L. M., 1987, Cross-hole tomography for strongly variable media with applications to scale model data: *Bull., Seis. Soc. Am.*, 77, 1945-1960.

Vesnaver, A. L., 1996, The contribution of reflected, refracted and transmitted waves to seismic tomography; a tutorial: *First Break* 14, 5, 159-168.